

# $\Lambda$ polarization in peripheral collisions at moderate relativistic energies

Y.L. Xie<sup>1</sup>, M. Bleicher<sup>2,3</sup>, H. Stöcker<sup>2,3</sup>, D.J. Wang<sup>4</sup>, and L.P. Csernai<sup>1</sup>

<sup>1</sup>*Institute of Physics and Technology, University of Bergen, Allegaten 55, 5007 Bergen, Norway*

<sup>2</sup>*Frankfurt Institute for Advanced Studies - Goethe University, 60438 Frankfurt am Main, Germany*

<sup>3</sup>*Institut für Theoretische Physik, Goethe University, 60438 Frankfurt am Main, Germany*

<sup>4</sup>*School of Science, Wuhan University of Technology, 430070, Wuhan, China*

(Dated: March 6, 2024)

The polarization of  $\Lambda$  hyperons from relativistic flow vorticity is studied in peripheral heavy ion reactions at FAIR and NICA energies, just above the threshold of the transition to the Quark-Gluon Plasma. Previous calculations at higher energies with larger initial angular momentum, predicted significant  $\Lambda$  polarization based on the classical vorticity term in the polarization, while relativistic modifications decreased the polarization and changed its structure in the momentum space. At the lower energies studied here, we see the same effect namely that the relativistic modifications decrease the polarization arising from the initial shear flow vorticity.

PACS numbers: 25.75.-q, 24.70.+s, 47.32.Ef

## I. INTRODUCTION

Relativistic heavy ion collisions allow to explore the properties of hot and dense QCD matter in the laboratory. Among the most prominent observables are the different kinds of transverse flow e.g. radial flow, directed flow, elliptical flow, and higher order flows. Hydrodynamics has been shown to provide direct access to these flow patterns.

In recent fluid dynamical models of relativistic heavy ion reactions, both different fluctuating modes and global collective processes lead to flow observables. It is important to separate or split the two types of flow processes from each other [1, 2]. This separation helps to precisely analyze both processes.

In peripheral heavy ion reactions, due to the initial angular momentum, the reaction shows a shear flow characteristics, leading to rotation [3] and even Kelvin-Helmholtz Instabilities (KHI) [4] in the reaction plane, due to the low viscosity Quark-Gluon Plasma. This possibility was indicated by high resolution Computational Fluid Dynamics calculations using the PICR method. The development of these processes was studied in 3+1 dimensional (3+1D) configurations that described the energy and momentum balance realistically [5]. The initial state model assumed transparency as well as stopping [6] due to strong attractive fields with accurate impact parameter and rapidity dependence in the transverse plane [7]. It assumed an initial inter-penetration of Lorentz contracted slabs (in most present models considered as CGC), and strong attractive coherent Yang-Mills fields act between these slabs, with large string tension (according to the color rope model [8]).

In a previous work the development of vorticity was studied under the conditions where the viscosity is estimated to have a minimum, so the viscous dissipation is small, [9, 10], and the spherical expansion is also smaller due to the lower pressure. Thus the initial local rotation, the vorticity drops slower.

In the PICR calculation [5], the dynamical initial state,

a Yang-Mills field theoretical model [7] was used as in ref. [11], and a longitudinal expansion lasting 4 fm/c from the initial impact was considered.

The classical weighted vorticity  $\Omega_{zx}$ , was calculated in the reaction [x-z] plane, the energy of the Au+Au collision was  $\sqrt{s_{NN}} = 4.65 + 4.65$  GeV,  $b = 0.5b_{max}$ .

The used fluid dynamical calculation and this initial state model, has been tested in several model calculations in the last decade. It describes correctly the initial shear flow characteristics. The angular momentum distribution is based on the assumption that the initial angular momentum of the participants (based on straight propagation geometry) is streak by streak conserved, thus the model satisfies angular momentum conservation both locally and globally. Fig.1 shows the 3-dimensional view of the simulated collisions shortly after the impact, and it could naturally generate a longitudinal velocity shear along the  $x$  direction, as shown in Fig. 2(a). This type of longitudinal velocity shear is a requirement for the subsequent rotation, turbulence and even Kelvin Helmholtz instability(KHI), just as discussed in our previous paper[10], as well as in refs. [12, 13]. The vortical flow formed in the equilibrated hydro evolution, as shown in Figs. 2(b)(c)(d), can give rise to the polarization due to the equipartition principle or spin-orbit coupling.

The peak value of the vorticity at the energy  $\sqrt{s_{NN}} = 4.65 + 4.65$  GeV, was a few times smaller than at the ultra-relativistic RHIC and LHC energies, but the negative values are less pronounced. The initial state used is the same as the one that was used at high energy: we assume transparency, QGP formation, initial longitudinal expansion in the same Yang-Mills string rope model for 4 fm/c time. Besides, the frequently used ‘Bag Model’ EoS was also applied in the hydro simulation:  $P = c_0^2 e^2 - \frac{4}{3}B$ , where constant  $c_0^2 = \frac{1}{3}$  and  $B$  is the Bag constant in QCD [7, 14]. The energy density takes the form:  $e = \alpha T^4 + \beta T^2 + \gamma + B$ , where  $\alpha, \beta, \gamma$  are constants arising from the degeneracy factors for (anti-)quarks and gluons. At later time, the drop of the vorticity is not as

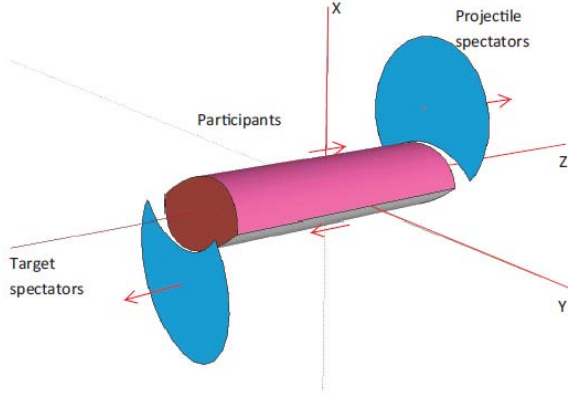


FIG. 1. (Color online) The three-dimensional view of the collisions shortly after the impact. The projectile spectators are going along the  $z$  direction; and the target spectators are going along the  $z$  axis. The collision region is assumed to be a cylinder with an almond-shaped profile and tilted end surfaces, where the top side is moving to the right and the bottom is moving to the left. The participant cylinder can be divided into streaks, and each streak has its own velocity, as shown in Fig. 2(a). The velocity differences among the streaks result in rotation, turbulence and even KHI.

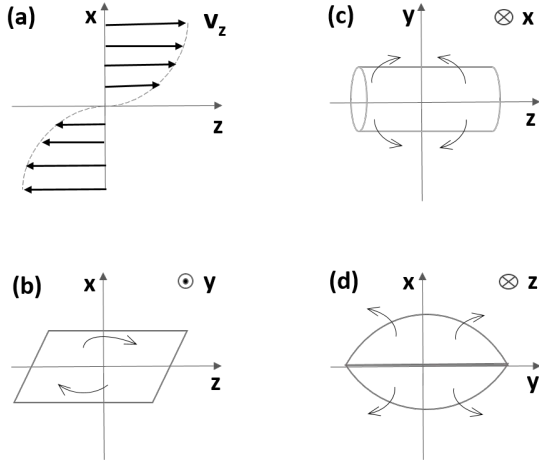


FIG. 2. (Color online) The schematic hydro flow velocity after the collisions shown in Fig. 1. Panel (a) is the longitudinal velocity profile along the  $x$  direction, and it gives rise to the  $v_1$  type of flow in the reaction plane, i.e. Panel (b). Panel (c) is the anti- $v_2$  type of flow in the  $[y-z]$  plane, and Panel (d) is the  $v_2$  type of flow in the  $[x-y]$  plane.

large as in higher energy heavy ion collisions.

In ref. [5] the classical and relativistic weighted vorticities,  $\Omega_{zx}$ , were evaluated in the reaction plane,  $[x-z]$ , so that the weighting does not change the average circulation of the layer, i.e., the sum of the average of the weights over all fluid cells is unity. The vorticity projected to the reaction plane for a collision for the FAIR-SIS300 energy of  $\sqrt{s_{NN}} = 8.0$  GeV is evaluated at an initial moment of

time and at a later time. The peak value of the vorticity is similar to the one obtained at the ultra-relativistic RHIC and LHC energies, but the negative values are less pronounced. The average vorticity was decreasing with time:  $\Omega_{zx}$  is 0.1297 / 0.0736 for the times,  $t = 0.17$  and 3.56 fm/c respectively. The same behavior was seen in ref. [15].

In addition to the directed flow ( $v_1$ ) [3, 16] two methods were proposed so far to detect the effects of rotation: the Differential HBT method [17] and the polarization of emitted fermions based on the equipartition of the rotation between the spin and orbital degrees of freedom [18, 19].

The particle polarization effect has some advantages and disadvantages. The local polarization depends on the thermal vorticity [18, 19]. Now at lower collision energy the temperature is lower and the thermal vorticity increases, which is advantageous. At ultra-relativistic energies this feature led to the conclusion that the predicted polarization is bigger for RHIC than for LHC, because of the lower temperature of the system. Furthermore at ultra-relativistic energies, the relativistic corrections to polarization will become stronger compared to the original shear and the resulting classical vorticity [20].

The thermal vorticity occurs in the particle polarization, because the spin-orbit interaction aligns the spins and the orbital momentum, while the random thermal motion works against this alignment. Thus, we use the inverse temperature four-vector field [18, 19],

$$\beta^\mu(x) = (1/T(x))u^\mu(x),$$

and define the *thermal vorticity* as:

$$\varpi^{\mu\nu} = \frac{1}{2}(\partial^\nu \hat{\beta}^\mu - \partial^\mu \hat{\beta}^\nu), \quad (1)$$

where  $\hat{\beta}^\mu \equiv \hbar \beta^\mu$ . Thereby,  $\varpi$  becomes dimensionless.

The relativistic weighted thermal vorticity  $\Omega_{zx}$ , calculated in the reaction  $[x-z]$  plane was presented in ref. [5]. The energy of the Au+Au collision was  $\sqrt{s_{NN}} = 4.65 + 4.65$  GeV, and the impact parameter  $b = 0.5b_{max}$ . The obtained average thermal vorticity,  $\Omega_{zx}$ , was 0.0847 (0.0739) for the times,  $t = 0.17$  and 3.56 fm/c respectively. It was observed that the thermal vorticity decreases slower than the standard vorticity due to the decreasing temperature.

In ref. [5] the relativistic weighted thermal vorticity  $\Omega_{zx}$ , was calculated in the reaction  $[x-z]$  plane at  $t = 0.34$  fm/c and at  $t = 3.72$  fm/c for the energy of the collision  $\sqrt{s_{NN}} = 4.0 + 4.0$  GeV,  $b = 0.5b_{max}$ .  $\Omega_{zx}$  was 0.0856 (0.0658) for the two selected times.

An analysis of the vorticity for peripheral Au+Au reactions at NICA and U+U reactions at FAIR energies of  $\sqrt{s_{NN}} = 9.3(8.0)$  GeV respectively gave an initial peak vorticity that was about two times larger than the one obtained from random fluctuations in the transverse plane, of about 0.2 c/fm at much higher energies [21]. This is due to the initial angular momentum arising from the beam energy in non-central collisions.

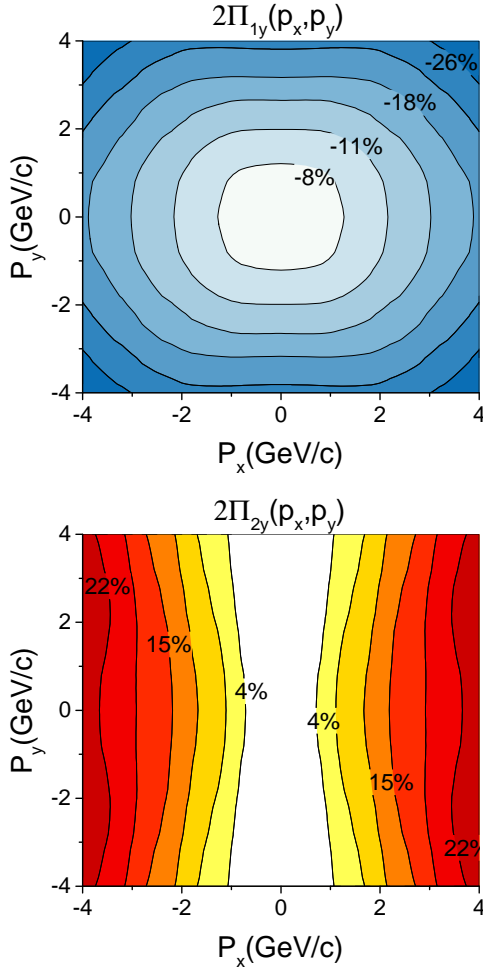


FIG. 3. (Color online) The first (top) and second (bottom) term of the dominant  $y$  component of the  $\Lambda$  polarization for momentum vectors in the transverse,  $[p_x, p_y]$ , plane at  $p_z = 0$ , for the FAIR U+U reaction at  $\sqrt{s_{NN}} = 8.0$  GeV.

The RHIC Beam Energy Scan program measured significant  $\Lambda$  and  $\bar{\Lambda}$  polarizations, with the largest values at the lowest energies [22].

At FAIR, the planned facilities, e.g. at PANDA [23], will make it possible to measure proton and anti-proton polarization, also in the emission directions where significant polarization is expected.

## II. POLARIZATION STUDIES

The flow vorticity was evaluated and reported in [5]. Based on these results we report the  $\Lambda$  polarization results for the same reactions. The initial state Yang-Mills flux-tube model [7] describes the development from the initial touching moment up to 2.5 fm/c. Then the PICR Hydro code is calculated for another 4.75 fm/c, so that the final freeze out time is 7.25 fm/c.

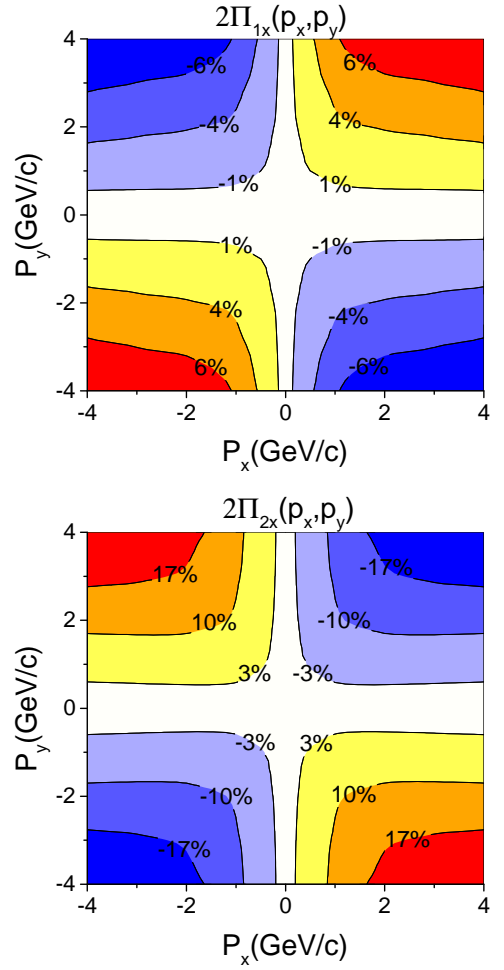


FIG. 4. (Color online) The first (top) and second (bottom) term of the  $x$  component of the  $\Lambda$  polarization for momentum vectors in the transverse,  $[p_x, p_y]$ , plane at  $p_z = 0$ , for the FAIR U+U reaction at  $\sqrt{s_{NN}} = 8.0$  GeV.

The  $\Lambda$  and  $\bar{\Lambda}$  polarization was calculated based on the work [19]

$$\begin{aligned} \Pi(p) = & \frac{\hbar \varepsilon}{8m} \frac{\int d\Sigma_\lambda p^\lambda n_F (\nabla \times \boldsymbol{\beta})}{\int d\Sigma_\lambda p^\lambda n_F} \\ & + \frac{\hbar \mathbf{p}}{8m} \times \frac{\int d\Sigma_\lambda p^\lambda n_F (\partial_t \boldsymbol{\beta} + \nabla \beta^0)}{\int d\Sigma_\lambda p^\lambda n_F}. \end{aligned} \quad (2)$$

where,  $n_F(x, p)$  is the Fermi-Jüttner distribution of the  $\Lambda$ , that is  $1/(e^{\beta(x) \cdot p - \xi(x)} + 1)$ , being  $\xi(x) = \mu(x)/T(x)$  with  $\mu$  the relevant  $\Lambda$  chemical potential and  $p$  its four-momentum.  $d\Sigma_\lambda$  is the freeze out hypersurface element, for  $t = \text{const.}$  freeze-out  $d\Sigma_\lambda p^\lambda \rightarrow dV \varepsilon$ , where  $\varepsilon = p^0$  being the  $\Lambda$ 's energy.

Here the *first term* is the classical vorticity term, while the *second term* is the relativistic modification. The above convention of  $\Pi(p)$  [19] is normalized to max. 50%, while in the experimental evaluation it is 100 %, thus we

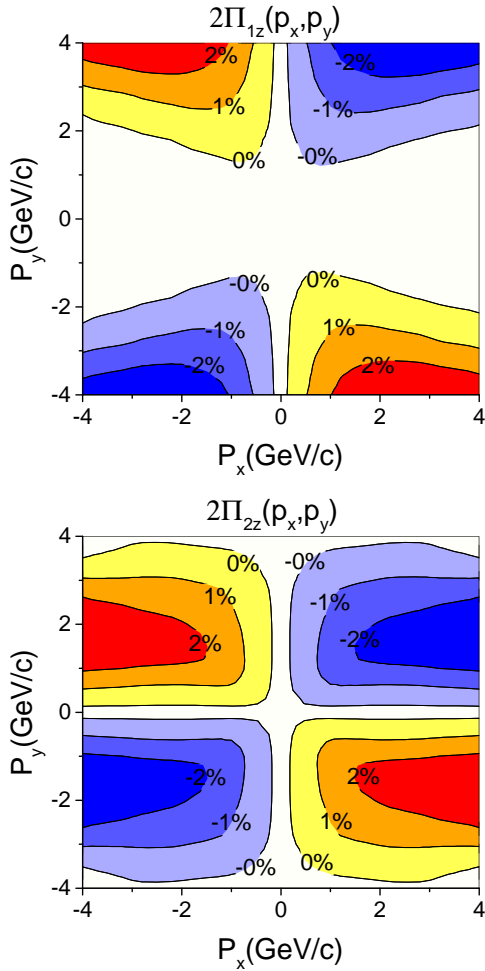


FIG. 5. (Color online) The first (top) and second (bottom) term of the  $z$  component of the  $\Lambda$  polarization for momentum vectors in the transverse,  $[p_x, p_y]$ , plane at  $p_z = 0$ , for the FAIR U+U reaction at  $\sqrt{s_{NN}} = 8.0$  GeV.

present the values of  $2\Pi(p)$ , [20] unlike in earlier calculations [18, 24, 25].

In Fig. 3 the dominant  $y$  component of the polarization vector  $\Pi(p)$ , for the first and second terms are shown. The first term is pointing into the negative  $y$  direction with a maximum of -26%. The structure of first term arises from the  $v_1$  type of flow in Fig. 2(b), which is also unipolar and negative  $y$  directed. The second term has different structure, it points in the opposite direction and has a maximum of +22%, i.e.  $\sim 4\%$  less than the absolute value of the first term.

In Fig. 4 the  $x$  component of the polarization vector  $\Pi(p)$ , for the first and second terms are shown. The first term is about four times smaller than the  $y$  component,  $\pm 6\%$ , and the positive and negative values are symmetric in a way that the integrated value of the polarization over the momentum space in the transverse plane is vanishing. This sign distribution is just the manifestation

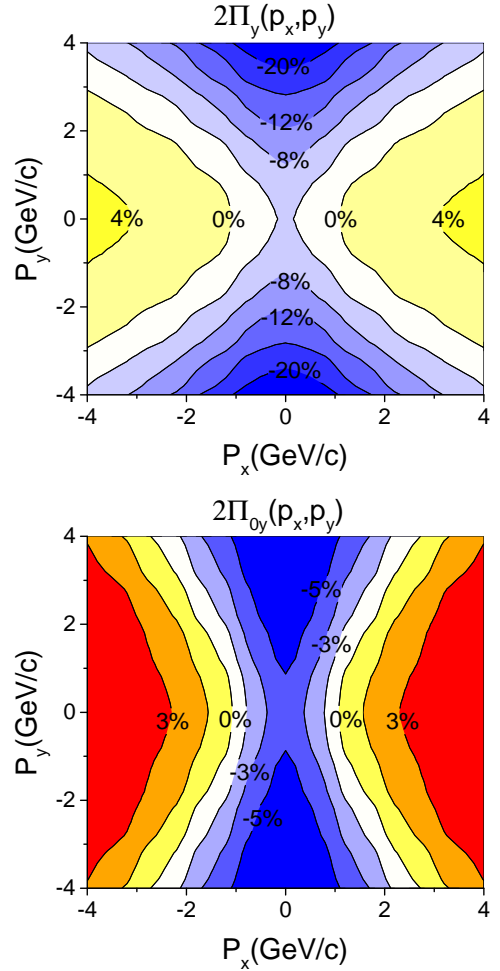


FIG. 6. (Color online) The  $y$  component of the  $\Lambda$  polarization for momentum vectors in the transverse,  $[p_x, p_y]$ , plane at  $p_z = 0$ , for the FAIR U+U reaction at  $\sqrt{s_{NN}} = 8.0$  GeV. The top figure is in the calculation frame, while the bottom figure is boosted to the frame of the  $\Lambda$  [18].

of anti- $v_2$  type of flow in  $[y-z]$  plane, seen in Fig. 2(c) with a dipole structure. The second term is about half of the  $y$  component,  $\pm 17\%$ , and the positive and negative values are symmetric in a way that the integrated value of the polarization over the momentum space in the transverse plane is vanishing. Furthermore the first and second terms have opposite signs at the same momentum values in the transverse plane, which decreases further their effect.

In Fig. 5 the  $z$  component of the polarization vector  $\Pi(p)$ , for the first and second terms are shown. The first term has a maximum of  $\pm 2\%$ , and the positive and negative values are symmetric in a way that the integrated value of the polarization over the momentum space in the transverse plane is vanishing. This sign distribution is also the manifestation of the anti- $v_2$  type of flow in  $[x-y]$  plane, i.e. a dipole structure in Fig. 2(d). The

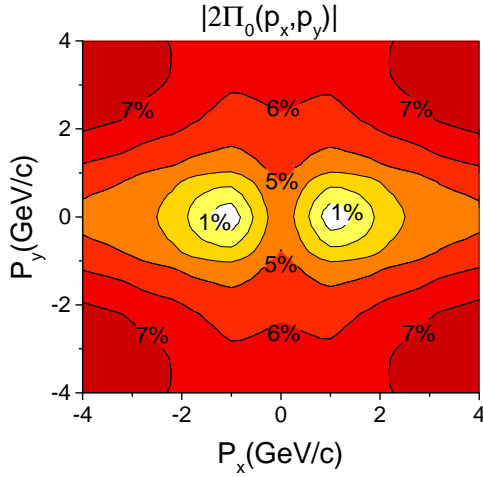


FIG. 7. (Color online) The modulus of the  $\Lambda$  polarization for momentum vectors in the transverse,  $[p_x, p_y]$ , plane at  $p_z = 0$ , for the FAIR U+U reaction at  $\sqrt{s_{NN}} = 8.0$  GeV. The figure is in the frame of the  $\Lambda$ .

second term has similar structure to the first one, with a maximum of  $\pm 2\%$  also, but the first and second terms have similar structure in the momentum space.

In Fig. 6 the dominant  $y$  component of the polarization vector  $\mathbf{\Pi}(p)$ , for the sum of the first and second terms is shown. The top figure is the distribution of the polarization in the center-of-mass frame while the bottom figure is in the local rest frame of the  $\Lambda$ .

Fig. 7 shows the modulus of the polarization vector  $\mathbf{\Pi}(p)$ . The maximum at high  $|p_y|$  and low  $|p_x|$  is the same as the absolute value of the  $\Pi_{0y}$  component. Here the other components have only minor contributions to the final observed polarization. At the corners, at high  $|p_y|$  and high  $|p_x|$ , the contribution of the  $x$  and  $z$  components of  $\mathbf{\Pi}(p)$  dominates, while the  $y$  component has a minimum.

Fig. 8 shows the  $y$  component and the modulus of the polarization vector  $\mathbf{\Pi}(p)$  for the NICA Au+Au reaction at  $\sqrt{s_{NN}} = 9.3$  GeV. The structure and magnitude of the polarization is similar to the reactions at FAIR. The negative maximum at high  $|p_y|$  and low  $|p_x|$  arises from the classical vorticity in the  $y$  component. The positive maximum at high  $|p_x|$  and low  $|p_y|$  arises from the relativistic modifications of the second term. The momentum space average is dominated by the first term.

The polarization studies at ultra-relativistic, RHIC and LHC energies, turned out to be sensitive to both the classical vorticity of the flow (first term) and the relativistic modifications arising from rapid expansion at later stages of the flow (second term) [18, 20].

Initially the contribution of the classical vorticity is stronger than the relativistic modification term, i.e. the 'second' term. This is in line with earlier observations [5, 15]. The effect of this decrease is also visible in the polarization results. The  $\Lambda$  polarization was evaluated at

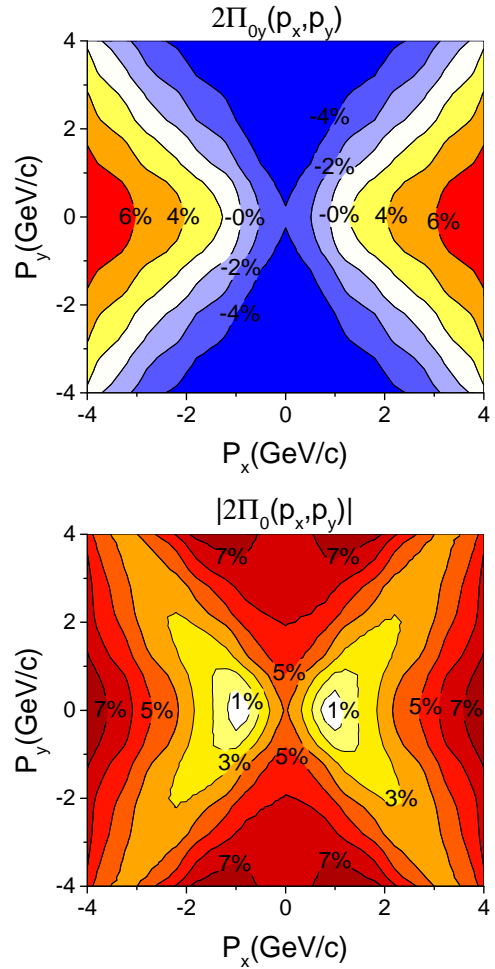


FIG. 8. (Color online) The  $y$  component (top) and the modulus (bottom) of the  $\Lambda$  polarization for momentum vectors in the transverse,  $[p_x, p_y]$ , plane at  $p_z = 0$ , for the NICA Au+Au reaction at  $\sqrt{s_{NN}} = 9.3$  GeV. The figure is in the frame of the  $\Lambda$ .

earlier freeze out time,  $t = 2.5 + 1.7\text{fm}/c = 4.2\text{fm}/c$  for the FAIR U+U reaction. See Fig. 9

The  $y$  component and the modulus of the polarization vector  $\mathbf{\Pi}(p)$  have very similar structure and magnitude, although the  $y$  component points in the negative  $y$  direction as the angular momentum vector from the initial shear flow. This indicates that the other,  $x$  and  $z$ , components are of the order of 1% only at moderate momenta where the  $y$  component and the modulus are of the order of 5-6%. At the "corners", at high  $|p_y|$  and high  $|p_x|$ , the contribution of the  $x$  and  $z$  components of  $\mathbf{\Pi}(p)$  are approaching that of the  $y$  component, so that the modulus is larger than the  $y$  component, by 4-5%. Still the contribution of these second term components is clearly smaller than the classical vorticity component.

It is important to mention the role of the initial condition. The *second term*, the relativistic modification, develops during the expansion of the system and is not

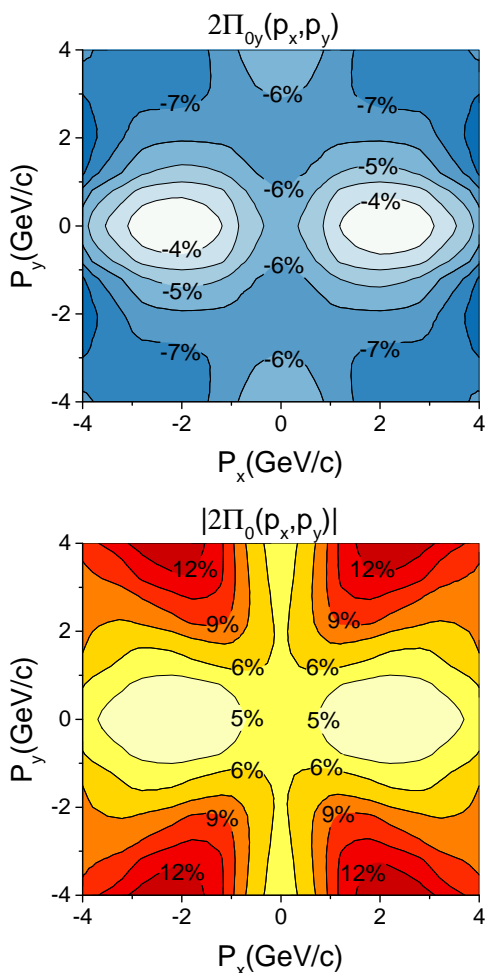


FIG. 9. (Color online) The  $y$  component (top) and the modulus (bottom) of the  $\Lambda$  polarization for momentum vectors in the transverse,  $[p_x, p_y]$ , plane at  $p_z = 0$ , for the FAIR U+U reaction at  $\sqrt{s_{NN}} = 8$  GeV at the earlier freeze out time of  $t = 4.2$  fm/c. The figure is in the frame of the  $\Lambda$ .

very sensitive to the initial state. This is shown by the fact that the structure of the  $x$  component of polarization,  $\Pi_{2x}$  in the dominant Fig. 4b, is very similar to Fig. 14b of ref. [25]. At the same time here the initial shear and classical vorticity are present in the initial state with strong stopping and dominance of the Yang-Mills field, [6, 7], while in ref. [25] this is not present. As a consequence the final polarization estimates in the  $y$  direction are different in the two models.

### III. TOTAL $\Lambda$ POLARIZATION INTEGRATED OVER MOMENTUM SPACE

Since the experimental results for  $\Lambda$  polarization are averaged polarizations over the  $\Lambda$  momentum, we evaluated the average of the  $y$  component of the polarization

$\langle \Pi_{0y} \rangle_p$ . We integrated the  $y$  component of the obtained polarization,  $\Pi_{0y}$ , over the momentum space as follows:

$$\begin{aligned} \langle \Pi_{0y} \rangle_p &= \frac{\int dp dx \Pi_{0y}(p, x) n_F(x, p)}{\int dp dx n_F(x, p)} \\ &= \frac{\int dp \Pi_{0y}(p) n_F(p)}{\int dp n_F(p)} \end{aligned} \quad (3)$$

For Au+Au collisions at NICA energy (9.3 GeV/A), the averaged  $y$  component of polarization is 1.82%, at freeze out time 2.5+4.75 fm/c, while for the U+U collisions at FAIR energy (8 GeV/A) at the same time, the value is 1.85%, a bit larger. As some papers [18, 26] had pointed out, the  $\Lambda$  polarization scales with  $x_F = 2p/\sqrt{s}$ , thus the  $\Lambda$  polarization should increase with decreasing energy, which is also, more or less, being confirmed by our results. We also evaluated the average polarization for U+U collisions at 8 GeV/A energy at an earlier time 2.5+1.7 fm/c, and the obtained value is about 2.02%, showing that the average polarization is decreasing with freeze out time.

It is important to mention that if vorticity and polarization are dominated by the expansion and not by the initial shear flow then the vorticity is symmetric, see Fig. 13 of ref. [25], and the polarization also as shown in Fig. 4b, and similarly in Fig. 14b of ref. [25]. Due to the symmetry of the polarization in the  $\pm$  directions these polarizations average out to zero. This applies to the  $y$  directed polarization in the model initial state of ref. [25] also. The result that the present model yields to a net average polarization,  $\Pi_{0y}$ , in the negative  $y$  direction, is due to the strong shear flow and vorticity in the initial state.

The vorticity induced by the initial orbital angular momentum will eventually give rise to non-vanishing local and global polarization, which is aligned with the initial angular momentum [12, 13, 27–31]. As eq. (4.4) in Ref. [12] shows, the quark polarization rate is sensitive to the viscosity,  $\eta/s$ . This equation also indicates that the modulus of quark polarization is inversely proportional with the center-of-mass energy. On the other hand, this equation is based on the one-dimensional Bjorken assumption, i.e. the transverse expansion was not considered, while in our model the spherical expansion is manifested in the second term, and obviously influences the final polarization significantly.

Previous experimental results, e.g. Au+Au collisions at 62.4 GeV and 200 GeV in RHIC, have shown global polarization [32], with large error bars. We have to point out that these experiments had a centrality percentage of 0-80% in RHIC, which dilutes the obtained polarization values after averaging. Also the azimuth averaged values are much smaller than values for given azimuthal ranges as shown in Fig. 8. Furthermore Fig. 2 in Ref. [28] and Fig. 3 in Ref. [33] have shown a centrality region of nontrivial initial angular momentum, which drops drastically above 50% and below 20% centrality percentage. Since the polarization originates from initial angular momentum, it is better to measure the polarization effect in



the 20%-50% centrality percentage range. The centrality percentage value used in our model is 30%, which gives us the peak value of initial angular momentum.

For the correct determination of the momentum space dependence of  $\Lambda$  polarization, we have to know the reaction plane and the Center of Mass (CM) of the participant system in a peripheral heavy ion reaction. The Event by Event (EbE) determination of the longitudinal CM of participants could be measured by the forward backward asymmetry of the particles in the Zero Degree Calorimeters (ZDCs). In colliders only single neutrons are measured in the ZDCs, so one has to extrapolate from these to the total spectator momenta. This method to detect the EbE CM was proposed in Refs. [1, 34].

At collider experiments, e.g. the LHC-ALICE or RHIC-STAR, this determination was not performed up to now, with the argument [35] that nuclear multi-fragmentation may also lead to fluctuation of single neutron hits in ZDCs, and therefore CM frame would have been determined inaccurately. However, at FAIR's fixed target experiments, it is possible to detect all the fragments from multi-fragmentation of spectators, thus the CM frame can be determined accurately.

Since the experimental measurement of global  $\Lambda$  polarization is conducted around different azimuthal angle, it is crucial to accurately define the EbE CM frame. In symmetric collider experiments, the CM frame de facto fluctuates around the actual CM frame. The fixed target FAIR setup can get rid of this uncertainty perfectly. The

Compressed Byronic Matter (CBM) experiments will be able to measure the polarization effects at SIS-100 and SIS-300 with millions times higher intensity and event rate, up to six order of magnitude than at the RHIC Beam Energy Scan program.

The higher multiplicity, thus allows for the high resolution measurement of the momentum space dependence of the  $\Lambda$  polarization, which can be decisive to determine the dominant polarization mechanism.

#### IV. SUMMARY

We have explored  $\Lambda$  polarization as an observable signal for the vorticity created in peripheral heavy ion collisions. The studies were performed within a (3+1D) hydrodynamic simulation for U+U collisions at FAIR energies ( $\sim \sqrt{s_{NN}} = 8$  GeV). We predicted a sizeable polarization signature in the emitted  $\Lambda$  hyperons that can directly signal the initial vorticity. The predictions can be explored at the NICA and FAIR facilities in the near future.

#### ACKNOWLEDGMENTS

Enlightening discussions with Francesco Becattini are gratefully acknowledged. This work was partially supported by the Helmholtz International Center for FAIR within the Hessian LOEWE initiative.

- 
- [1] L. P. Csernai and H. Stöcker, J. Phys. G **41**, 124001 (2014).
  - [2] S. Floerchinger and U.A. Wiedemann, Phys. Rev. C **88**, 044906 (2013).
  - [3] L. P. Csernai, V. K. Magas, H. Stöcker, and D. D. Strottman, Phys. Rev. C **84**, 024914 (2011).
  - [4] L. P. Csernai, D. D. Strottman and Cs. Anderlik, Phys. Rev. C **85**, 054901 (2012).
  - [5] L. P. Csernai, D. J. Wang, M. Bleicher, and H. Stöcker, Phys. Rev. C **90**, 021904(R) (2014).
  - [6] L. P. Csernai and J. I. Kapusta, Phys. Rev. D **31** 2795 (1985).
  - [7] V. K. Magas, L. P. Csernai, and D. D. Strottman, Phys. Rev. C **64**, 014901 (2001); and V. K. Magas, L. P. Csernai, and D. D. Strottman, Nucl. Phys. A **712**, 167 (2002).
  - [8] T. S. Biró, H. B. Nielsen, and J. Knoll, Nucl. Phys. B **245**, 449 (1984).
  - [9] P. K. Kovtun, D. T. Son and A. O. Starinets, Phys. Rev. Lett. **94**, 111601 (2005).
  - [10] L. P. Csernai, J. I. Kapusta, L.D. McLerran, Phys. Rev. Lett. **97**, 152303 (2006).
  - [11] L. P. Csernai, V. K. Magas, and D. J. Wang, Phys. Rev. C **87**, 034906 (2013).
  - [12] X.-G. Huang, P. Huovinen, and X.-N. Wang, Phys. Rev. C **84**, 054910 (2011).
  - [13] Z.-T. Liang and X.-N. Wang, Phys. Lett. B **629**, 20-26 (2005).
  - [14] L. P. Csernai, Introduction to Relativistic Heavy Ion Collisions, (Jonh Wiley & Sons Ltd., Chichester, 1994).
  - [15] Y. Jiang, Z.-W. Lin, and J.-F. Liao, arXiv:1602.06580v1.
  - [16] J. Steinheimer, J. Auvinen, H. Petersen, M. Bleicher, H. Stöcker, Phys. Rev. C **89** 054913 (2014).
  - [17] L. P. Csernai, S. Velle and D. J. Wang, Phys. Rev. C **89**, 034916 (2014); L. P. Csernai, and S. Velle, Int. J. Mod. Phys. E **23**, 1450043 (2014).
  - [18] F. Becattini, L. P. Csernai, and D. J. Wang, Phys. Rev. C **88** 034905 (2013).
  - [19] F. Becattini, V. Chandra, L. Del Zanna, and E. Grossi, Annals of Phys. **338**, 32 (2013).
  - [20] F. Becattini, L. P. Csernai, D. J. Wang, and Y. L. Xie, Phys. Rev. C **93**, 069901(E) (2016).
  - [21] S. Floerchinger and U. A. Wiedemann, Journal of High Energy Physics, **11**, 100 (2011); and J. Phys. G: Nucl. Part. Phys. **38**, 124171 (2011).
  - [22] M. A. Lisa *et al.* (STAR Collaboration), Invited talk presented at the QCD Chirality Workshop 2016, Feb. 23-26, 2016, Los Angeles, USA.
  - [23] A. Dbeyssi, Time-like proton form factors and heavy lepton production at the PANDA experiment, Proceedings of Science, (Bormio 2013) 059.

- [24] Y. L. Xie, R. C. Glastad, and L. P. Csernai, Phys. Rev. C **92**, 064901 (2015).
- [25] F. Becattini, G. Inghirami, V. Rolando, A. Beraudo, L. Del Zanna, A. De Pace, M. Nardi, G. Pagliara, and V. Chandra, Eur. Phys. J. C **75**, 406 (2015).
- [26] A. M. Smith *et al.* (R608 Collaboration), Phys. Lett. B **185**, 209 (1987).
- [27] J.-H. Gao, Z.-T. Liang, S. Pu, Q. Wang, and X.-N. Wang, Phys. Rev. Lett. **109**, 232301 (2012).
- [28] J.-H. Gao, S.-W. Chen, W.-T. Deng, and Z.-T. Liang, Q. Wang, and X.-N. Wang, Phys. Rev. C **77**, 044902 (2008).
- [29] Z.-T. Liang and X.-N. Wang, Phys. Rev. Lett. **94**, 102301 (2005).
- [30] F. Becattini and F. Piccinini, Annals of Physics **323**, 2452-2473 (2008).
- [31] L.-G. Pang, H. Petersen, Q. Wang, X.-N. Wang, arXiv:1605.04024.
- [32] STAR Collaboration, B. I. Abelev *et al.*, Phys. Rev. C **76**, 024915 (2007).
- [33] F. Becattini, F. Piccinini, and J. Rizzo, Phys. Rev. C **77**, 024906 (2008).
- [34] L. P. Csernai, G. Eyyubova, and V. K. Magas, Phys. Rev. C **86**, 024912 (2012).
- [35] J. Schukraft (private communication).